Salt-Assisted Deposition of SnO_2 on α-MoO_3 Nanorods and Fabrication of Polycrystalline SnO_2 Nanotubes

Bin Liu and Hua Chun Zeng*

Department of Chemical and Environmental Engineering, Faculty of Engineering, and Chemical and Process Engineering Center, National University of Singapore, 10 Kent Ridge Crescent, Singapore 119260

Received: December 11, 2003; In Final Form: March 8, 2004

Rutile-like tin dioxide (SnO_2; tetragonal symmetry) is a strategic material for a wide range of important applications. Although numerous methods have been developed for preparations of SnO_2 nanoparticles, nanowires, and nanorods, there has been no rational synthetic method reported to prepare this functional material into tubular nanostructures. In this article, we describe a facile template method for synthesis of free-standing polycrystalline SnO_2 nanotubes in aqueous solution. With soluble α-MoO_3 nanorod templates, polycrystalline SnO_2 can be first deposited under normal atmospheric pressure (room temperature to 100 °C) or hydrothermal conditions (180 °C). In particular, salt additives such as Na_2SO_4 have been proven to be indispensable for the deposition of SnO_2 skins. Various preparative parameters have been examined in detail, and dissolution modes of α-MoO_3 have also been investigated to address the formation mechanism. The optical band gap determined for the nanotubes is 3.92 eV (for crystallites with an average size of ∼4 nm). This salt-assisted "one-pot" method promises large-scale production of polycrystalline SnO_2 nanotubes with both structural engineering and crystallite size control.

Introduction

In recent years, functional monometal oxides have received increasing attention in the synthesis of nanostructured materials.[1−4] Among them, tetragonal tin dioxide (with rutile-like structure), SnO_2, is one of the most important strategic materials used in a wide range of technological applications.[5−39] This wide band gap n-type semiconductor ($E_g = 3.62$ eV, at room temperature) possesses outstanding chemicophysical properties for practical uses such as optoelectronic devices (e.g., LEDs), gas sensors, photocatalysts, nanofiltration membranes, heat mirrors, glass coatings, electrochromic windows, transparent electrodes for solar cells, and anode materials for lithium batteries. Various structural and morphological forms of SnO_2 nanomaterials have been fabricated over the past several years, including nanoparticles,[5−16] nanowires,[17−20] nanoribbons,[21−25] nanorods,[26−30] nanodiskettes,[31,32] nanocomposites,[33−35] and mesoporous powders and thin films.[36−39]

In contrast to the many investigations on the low-dimensional structures mentioned above, the synthesis of SnO_2 nanotubules has not received great attention. Perhaps due to a lack of practical synthetic methods and processing techniques, there is only one report on the fabrication of SnO_2 nanotubes to date. This study involved high-temperature, low-pressure conditions (1100 °C and 250 Torr).[28] It has been found that in addition to a main rutile phase, orthorhombic phase is also formed on the surface region of the SnO_2 nanotubes. Furthermore, the internal cavity of the tubes is not always continuous throughout the length, indicating the difficulty of controlling this process. Despite this, the reported vapor approach stands as the first pioneering synthesis of single-crystalline SnO_2 nanotubes.[28]

Inspired by carbon and inorganic fullerene-like nanotubes such as BN, MoS_2, and WS_2,[40−44] it is highly desirable to develop rational synthetic methods for SnO_2 nanotubes. For example, the inner "nanospace" and external surface of SnO_2 nanotubes may create different chemical environments for different chemical processes; the nanotube itself can be treated as a "nanoreactor" in the context of chemical reactions. Apart from the single-crystalline SnO_2 nanotubes, furthermore, controllability of crystallite size and texture of the SnO_2 nanotubes represents another technological challenge in nanotube fabrication, as polycrystalline nanotubes could be even more useful considering their chemical reactivity, surface usage, durability, reusability, quantum confinement effects, etc. For example, small SnO_2 crystallites in the polycrystalline tube walls might become even more tolerant to intercalant species to withstand harsh intercalation−deintercalation cycles.

Herein we describe a facile solution method for the synthesis of free-standing tetragonal SnO_2 nanotubes at room temperature to 180 °C. In particular, polycrystalline SnO_2 walls can be first deposited on α-MoO_3 nanorod templates, which is followed by dissolution of α-MoO_3 templates. This "one-pot" method also allows us to have structural engineering and crystallite texture control for the large-scale preparation of the SnO_2 nanotubes.

Experimental Section

Hydrothermal Preparation. In a typical experiment listed in Table 1, 0.02−0.10 g of α-MoO_3 nanorods (the synthesis of α-MoO_3 nanorods has been detailed in our previous report[45]) and 0−3.0 g of Na_2SO_4 salt (>99%, Merck) were added to 30−40 mL of deionized (DI) water. A 4 M HNO_3 solution (0−4 mL) was used to acidify the above solid−solution mixture. The mixture was kept in an ultrasonic water bath for 5 min in order to disperse the α-MoO_3 nanorods, after which 0.1−0.25 g of $SnCl_2 \cdot 2H_2O$ was added. The mixture was then transferred to a Teflon-lined stainless steel autoclave and placed inside an electric oven at 180 °C for 4−24 h. After the reactions, the

* To whom correspondence should be addressed. E-mail: chezhc@nus.edu.sg.

10.1021/jp037822d CCC: $27.50
Published on Web 04/16/2004

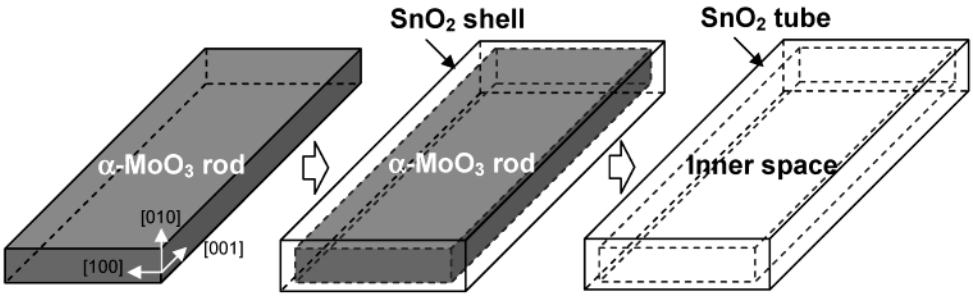

Figure 1. Schematic illustration of synthetic process of plateletlike SnO_2 nanotubes using soluble α-MoO_3 nanorod templates. Note that the geometric structure of the nanotubes can be predesigned by the α-MoO_3 templates.

TABLE 1: Summary of Experimental Procedures and Product Morphologies

type	experimental procedure	temp/time	product morphology
without Na_2SO_4	0.10 g of α-MoO_3 nanorods + 30−40 mL of H_2O + 1−3 g of Na_2SO_4 + 1−1.5 mL of HCl (4 M) + 0.2 g of $SnCl_2{\cdot}2H_2O$	100−180 °C/4 h; cooled to 25 °C within 20 h	SnO_2 nanoparticles
with Na_2SO_4	0.02−0.10 g of α-MoO_3 nanorods + 30−40 mL of H_2O + 1−3 g of Na_2SO_4 + 1−8 mL of HNO_3 or HCl (4 M) + 0.1−0.5 g of $SnCl_2{\cdot}2H_2O$	180 °C/4−24 h	SnO_2 sheathed α-MoO_3 nanorods to pure SnO_2 nanotubes with crystallite size control
with Na_2SO_4 but without acid	0.10 g of α-MoO_3 nanorods + 30 mL of H_2O + 1 g of Na_2SO_4 + 0.2 g of $SnCl_2{\cdot}2H_2O$	180 °C/20 h	SnO_2 sheathed α-MoO_3 nanorods to pure SnO_2 nanotubes; with large rodlike crystallites on the tube surfaces
with Na_2SO_4	0.10 g of α-MoO_3 nanorods + 2.0 g of Na_2SO_4 + 40−50 mL of DI water + 1.5−2.0 mL of HCl or HNO_3 (4 M) + 0.2 g of $SnCl_2{\cdot}2H_2O$	25 °C/24 h or 100 °C/4 h	SnO_2 sheathed α-MoO_3 nanorods[a]
with C_2H_5COONa	0.10 g of α-MoO_3 nanorods + 2.0 g of C_2H_5COONa + 50 mL of DI water + 2.0 mL of HCl (4 M) + 0.2 g of $SnCl_2{\cdot}2H_2O$	25 °C/24 h	SnO_2 sheathed α-MoO_3 nanorods, together with SnO_2 nanoparticles
with $NaNO_3$	0.10 g of α-MoO_3 nanorods + 2.0 g of $NaNO_3$ + 50 mL of DI water + 2.0 mL of HCl (4 M) + 0.2 g of $SnCl_2{\cdot}2H_2O$	25 °C/24 h	SnO_2 nanoparticles

[a] Pure SnO_2 nanotubes can be obtained after removal of α-MoO_3 templates in NaOH solution.

autoclave was either cooled under tap water or cooled naturally at room temperature. The solid products (i.e., SnO_2 nanotubes) were separated from the liquid phase via centrifugation and washed with deionized water (several times) and pure ethanol (one time), respectively. The final SnO_2 nanotubes and their related samples were then dried in a vacuum desiccator at room temperature overnight for materials characterization.

Preparations at Normal Atmospheric Pressure. In addition to the above hydrothermal method, preparations of SnO_2 nanotubes were also carried out at normal atmospheric pressure over a temperature range of 25−100 °C. In this type of synthesis, 0.1 g of α-MoO_3 nanorods and 2.0 g of Na_2SO_4 (>99%, Merck), or C_2H_5COONa (>99%, Fisher), or $NaNO_3$ (99%, Merck) were added to 40−50 mL of deionized water. A 4 M HNO_3 or HCl solution (1.5−2.0 mL) was further added. The solid−solution mixture was kept in an ultrasonic water bath for 5 min, after which 0.2 g of $SnCl_2{\cdot}2H_2O$ was added immediately. The mixture was then transferred to a glass conical flask and kept stirring at room temperature for 24 h or in a silicon-oil bath at 100 °C for 4 h. The postgrowth treatments of the products (SnO_2 nanotubes) were the same as those used in the hydrothermal syntheses.

XRD Measurement. The crystallographic phases of SnO_2 and α-MoO_3 samples were determined by powder X-ray diffraction (XRD). The XRD patterns with diffraction intensity versus 2θ were recorded in a Shimadzu X-ray diffractometer (Model 6000) with Cu Kα radiation ($\lambda = 1.5406$ Å) from 10° to 80° at a scanning speed of 2° min^{-1}. X-ray tube voltage and current were set at 40 kV and 30 mA, respectively.[46]

TEM/SEM/EDX/HRTEM/EDX Measurements. Investigations of high-resolution analytical transmission electron microscopy and energy-dispersive X-ray spectroscopy (HRTEM/TEM/EDX) were carried out in Philips-CM200 FEG and JEM-2010 with an electron kinetic energy of 200 kV. The specimens for TEM/HRTEM imaging and selected area electron diffraction (SAED) studies were prepared by suspending solid samples in acetone. About 2−3 mg of sample was added into 3−4 mL of acetone in a small glass container that was then placed in an ultrasonic water bath and sonicated for 30−40 min. A drop of this well-dispersed suspension was placed on a carbon coated 200-mesh copper grid, followed by drying of the sample under ambient conditions before it was placed in the sample holder of the microscope.[46] Sample morphologies were also examined with a scanning electron microscope (SEM, JSM-5600LV), equipped with EDX for a large-scale compositional analysis of the samples.

UV−Visible Measurement. UV−visible absorption spectroscopy measurement was carried out on a Shimadzu UV-3101 PC scanning spectrometer using pure ethanol as reference. About 0.01 g of solid SnO_2 nanotubes was dispersed in 3.5 mL of pure ethanol. During the measurement, 2 drops of the dispersed solution were added to a quartz sample holder (length of path $l = 10$ mm) prefilled with 4 mL of pure ethanol, followed by the spectrum measurement immediately.[46]

Results and Discussion

Single-crystalline α-MoO_3 nanorod templates were prepared with a hydrothermal method described previously.[45] Such nanorod templates have an elongated morphology of [001] ≫ [100] > [010]. Figure 1 shows a synthetic flowchart of this work, in which the formation of SnO_2 shell and removal of α-MoO_3 nanorod templates take place in a consecutive sequence under "one-pot" synthetic conditions. The general appearance

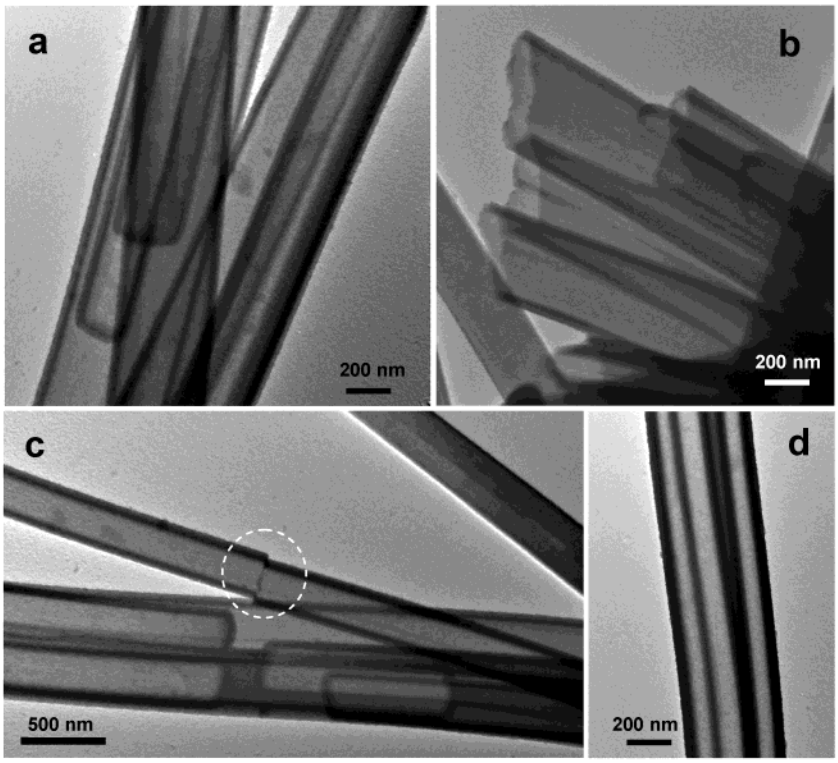

Figure 2. TEM images (a−d) of SnO_2 nanotubes synthesized in this work. The dashed circle indicates a cracking area. Synthetic conditions: 0.1 g of α-MoO_3 nanorods + 30 mL of H_2O + 1 g of Na_2SO_4 + 4 mL of HNO_3 solution (4 M) + 0.1 to 0.2 g of $SnCl_2 \cdot 2H_2O$ at 180 °C for 24 h.

of SnO_2 nanotubes prepared with this method is shown in Figure 2; note that the SnO_2 nanotubes retain the morphological shapes of templates which are about 100−400 nm in breadth, 50−100 nm in thickness, and several micrometers in length. There are two types of tube ending: closed ones (Figure 2a) and open ones (Figure 2b) that were generated from cracking of the tube (Figure 2c). In Figure 3, a detailed TEM investigation on a closed-ended tube is reported. The inner space and boundary lines have been investigated with a tilting examination (Supporting Information (SI), SI-1), which confirms the tubular structure. The walls of these nanotubes are comprised of nanocrystallites in sizes of around 4−5 nm (Figure 3c). Furthermore, the SAED pattern shown in Figure 3b indicates that the crystallites in the tubes are randomly oriented (i.e., polycrystalline), since only diffraction rings $(110)_s$, $(101)_s$, $(200)_w$, $(211)_s$, and $(112)_w/(301)_w$ (where s = strong, and w = weak) of the tetragonal phase SnO_2 can be observed.[15,17,34,35,39] Our TEM/SAED investigation on an open-ended tube is further reported in Figure 4. Results similar to those shown in Figure 3 were obtained. Once again, the nanocrystallites in this SnO_2 nanotube are randomly oriented, as evidenced in the diffraction rings of Figure 4b.[15,17,34,35,39] Consistent with this randomness, the deposition rates on different crystallographic planes of α-MoO_3 nanorods are essentially identical, which is reflected in the equal thickness of the SnO_2 shells observed (also refer to Figure 10b for the depositions on the {010} planes of α-MoO_3). It should be mentioned that the yield of SnO_2 nanotubes produced with this method is 100%, free of other morphological products of SnO_2.

The crystallographic phase information was investigated with powder XRD, which shows that the prepared SnO_2 nanotubes are in tetragonal symmetry (space group $P4_2/mnm$; $a_o = 4.74$ Å and $c_o = 3.19$ Å; JCPDS File No. 41-1445). In Figure 5, all diffraction peaks can be indexed perfectly to this crystal system. The broad peaks of this pattern indicate that the crystallites in the nanotubes are small. As confirmed in Figure 6, the crystallites within the nanotubes were well crystallized with a fairly uniform size (majority crystallites have an average crystallite size of around 5 nm). In particular, sharp lattice fringes with interplanar distances of $d_{220} = 0.17$ nm, $d_{202} = 0.13$ nm, and $d_{211} = 0.18$ nm can be easily observed, which is consistent with the found primary diffraction rings from the same families of crystal planes. The nanocrystallites of the nanotubes are indeed randomly oriented, including those in the edge portions. On the basis of HRTEM, it is further found that there are interparticulate spaces among the nanocrystallites (see SI-2). The formation of solid SnO_2 using the present precursors involves the following possible chemical reactions:[18,34,35]

$$SnCl_2 + 2H_2O \rightarrow SnO_2 + 2HCl + H_2 \quad (1)$$

$$2SnCl_2 + O_2 + 2H_2O \rightarrow 2SnO_2 + 4HCl \quad (2)$$

The O_2 required in eq 2 could be from dissolving oxygen in initial aqueous solutions or could be continuously supplied from a small amount of encapsulated air in the autoclave. The crystallite size of SnO_2 in the nanotubes can be further controlled via varying reaction conditions. For instance, larger crystallites can be obtained with a higher Sn^{2+}/α-MoO_3 ratio used in the synthesis (darker spots, Figure 4a). In such a case, some larger crystallites can be grown on the outer shells of the nanotubes after the initial growth. Nonetheless, the formation of SnO_2 still occurred strictly on the α-MoO_3 templates, and no spontaneous nucleation was observed even under these experimental conditions.

To understand the formation mechanism of the SnO_2 nanotubes, syntheses with a shorter reaction time were further carried out. Exemplified in Figure 7, the sheaths of SnO_2 were readily formed on the α-MoO_3 templates after only 4 h of reactions. Interestingly, cracking can be observed easily along the SnO_2 sheaths where the underneath α-MoO_3 becomes naked. Related to those in Figure 2b,c, it is now understood that the cracked

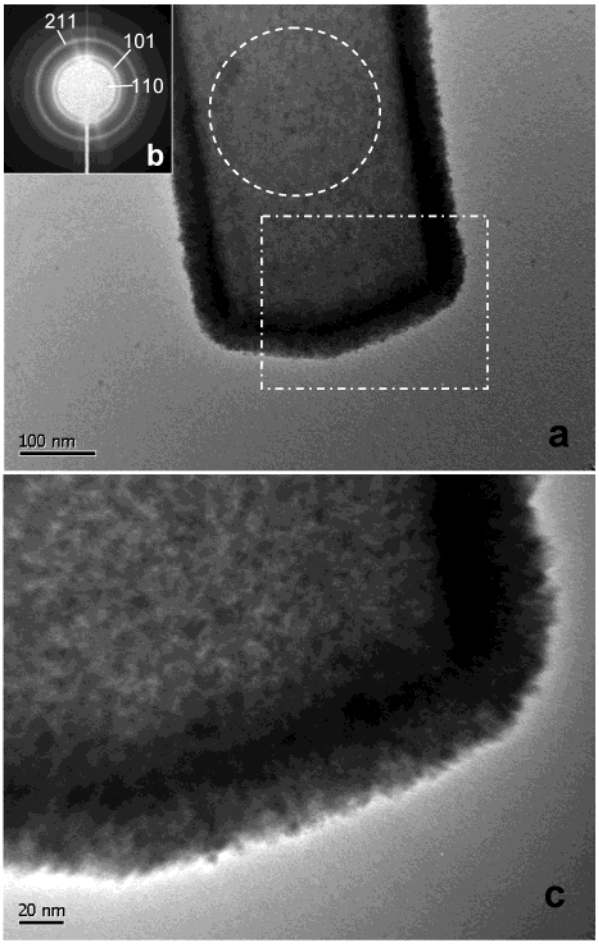

Figure 3. TEM and SAED investigations on a closed-ended SnO_2 nanotube: (a) end portion; (b) SAED pattern of the circled part of (a); (c) detailed view on the framed part of (a). Synthetic conditions: 0.1 g of α-MoO_3 nanorods + 30 mL of H_2O + 1 g of Na_2SO_4 + 4 mL of HNO_3 solution (4 M) + 0.2 g of $SnCl_2 \cdot 2H_2O$ at 180 °C for 24 h.

areas of the SnO_2 sheaths serve as primary starting points for the removal of α-MoO_3. Since the SnO_2 sheaths form within the first 4 h of the synthesis, it is reasonable to assume that the apparently longer reaction time required for the formation of the structures shown in Figures 2 and 3 was due primarily to the extra time needed for α-MoO_3 dissolution. There are three modes for this removal. As shown in Figure 8, depletion of α-MoO_3 takes place along {100} planes (e.g., Figure 8a,c). At the same time, the depletion can also occur primarily on {001} planes (e.g., Figure 8b,d). It is noted that the dissolution of α-MoO_3 is a slow hydrolysis process, resulting in formation of various soluble isopolymolybdate anions (including their polymeric species), such as $Mo_8O_{26}^{4-}$, $Mo_7O_{24}^{6-}$, $Mo_2O_7^{2-}$, and MoO_4^{2-},[47,48] according to an increase in the final pH value of a solution system. For instance, the commonly known heptamolybdate anion $Mo_7O_{24}^{6-}$ is stable at pH ≈ 4.5−6.0:[45]

$$7MoO_3 + 3H_2O \rightarrow Mo_7O_{24}^{6-} + 6H^+ \qquad (3)$$

For most of our experiments, the measured pH of final solutions after reactions fell in the range of 0.5−1.6, depending on the initial chemical combination and processing time chosen in synthesis. On the basis of eq 3, it is known that an acidic condition will shift the reaction to the left, slowing down the α-MoO_3 dissolution (common ion effect, i.e., H^+ ions in this equilibrium). Indeed, these pH data (i.e., acidic condition) indicate that a slow formation rate of SnO_2 and an even slower dissolution rate of α-MoO_3 templates had been realized under the studied conditions. In Figure 8d, the hollow part of an evacuated nanotube gives a polycrystalline diffraction pattern of SnO_2 while the sheathed part shows a superimposition of the same polycrystalline rings (i.e., SnO_2 shell)[15,17,34,35,39] and a sharp diffraction pattern ([010] zone diffraction spots) of single-crystalline α-MoO_3 (space group *Pbnm*; orthorhombic symmetry with lattice constants of $a_o = 3.9630$ Å, $b_o = 13.856$ Å, $c_o = 3.6966$ Å; basal spacing $d_{010}/2 = b_o/2$) owing to the composite nature of the sheathed structure (SnO_2−MoO_3). In good agreement with the phase analysis, our EDX investigation shows that both the SnO_2 shell and undissolved α-MoO_3 templates are in stoichiometric compositions (atomic ratios of Sn:O ≈ 1:2 and Mo:O ≈ 1:3) and free of contamination (see SI-3). In addition to α-MoO_3, however, H_xMoO_3 phase (also in orthorhombic symmetry, $x = 0.3$)[48] was detected (see SI-4), which indicates that α-MoO_3 templates also participate in the oxidation of $SnCl_2$ addition to eqs 1 and 2.

In principle, apart from the control of α-MoO_3 dissolution, the acid HNO_3 (or HCl) added in the synthesis also reduces the formation rate of solid SnO_2, which in turn allows us to further engineer shell textures via adjusting pH values [i.e., H^+ in eqs 1 and 2]. The formation rate of SnO_2 might be even slower with HCl, since Cl^- ions brought in by HCl will shift the reaction equilibria of eqs 1 and 2 to the left owing to common ion effects. Without using the acids, on the other hand, granulated and/or elongated SnO_2 crystallites can be prepared on the shells of the nanotubes while the α-MoO_3 templates are readily dissolved. This type of growth is illustrated in Figure 9, noting that discrete diffraction spots now appear clearly on the diffraction rings of tetragonal phase SnO_2 due to the presence of the large crystallites.[15,17,34,35,39] Regarding the shell formation, it is recognized that there is a large lattice mismatch between

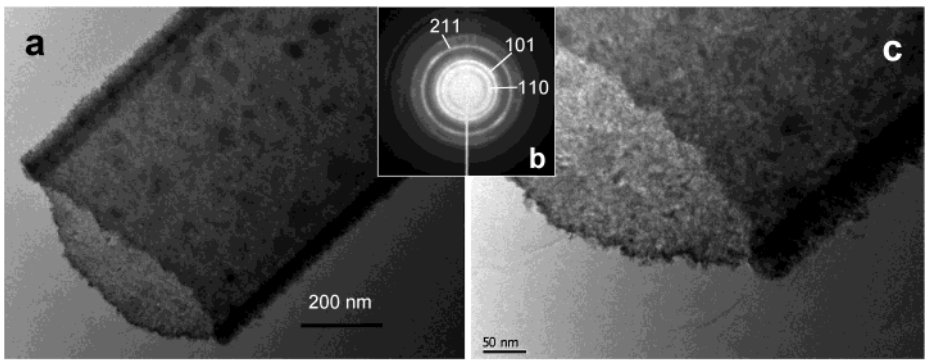

Figure 4. TEM and SAED investigations on an open-ended SnO_2 nanotube: (a) end opening; (b) SAED pattern of the middle portion of this tube; (c) detailed view on the end part of (a). Synthetic conditions: 0.02 g of α-MoO_3 nanorods + 40 mL of H_2O + 1 g of Na_2SO_4 + 1 mL of HNO_3 solution (4 M) + 0.25 g of $SnCl_2 \cdot 2H_2O$ at 180 °C for 24 h.

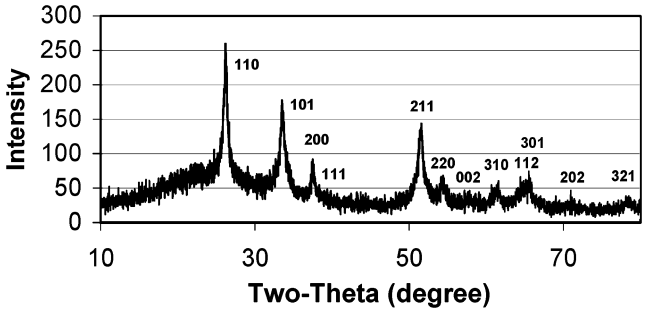

Figure 5. Representative XRD pattern of tetragonal phase SnO_2 nanotubes prepared in this work (sample from Figure 4). The background over 2θ range (10°−40°) is due to the signal generated from a glass sample holder used.

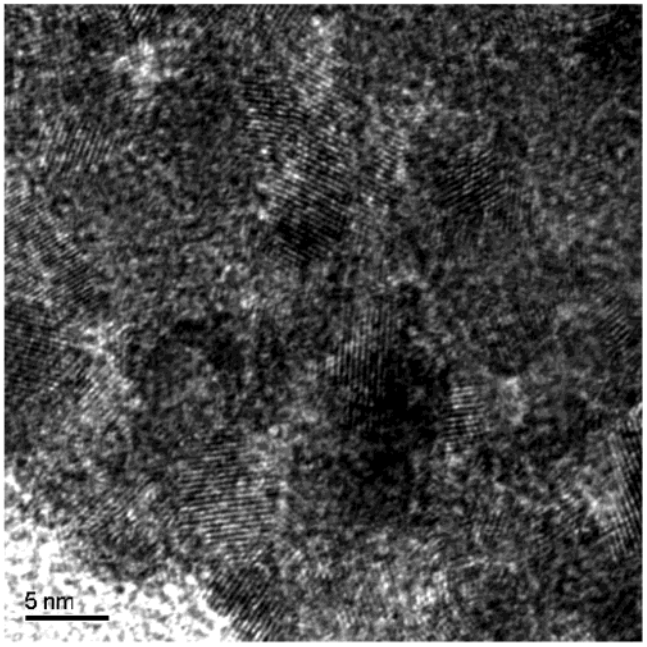

Figure 6. Representative HRTEM image on crystallite structure of SnO_2 nanotubes. Synthetic conditions: 0.02 g of α-MoO_3 nanorods + 40 mL of H_2O + 1 g of Na_2SO_4 + 1 mL of HNO_3 solution (4 M) + 0.25 g of $SnCl_2{\cdot}2H_2O$ at 180 °C for 24 h.

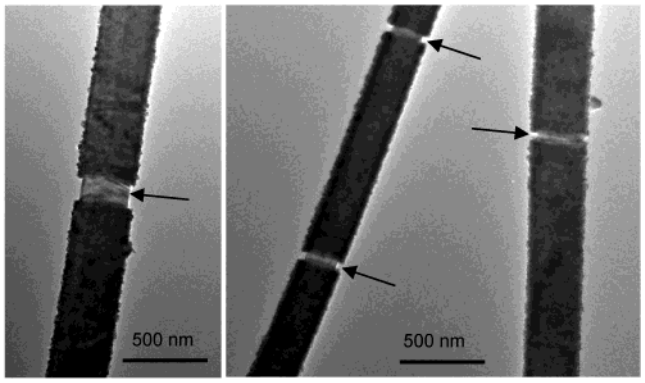

Figure 7. Representative HRTEM images of SnO_2 sheathed α-MoO_3 nanorods. Synthetic conditions: 0.1 g of α-MoO_3 nanorods + 30 mL of H_2O + 1 g of Na_2SO_4 + 1 mL of HCl solution (4 M) + 0.2 g of $SnCl_2{\cdot}2H_2O$ at 180 °C for 4 h. Arrows indicate the cracking areas of the SnO_2 skins and naked α-MoO_3 nanorods.

the deposited SnO_2 and α-MoO_3 substrate, which leads to a random heterogeneous nucleation of the overlayer. As individual crystallite sizes are much smaller than the shell thickness, the subsequent growth will take place via homogeneous nucleation

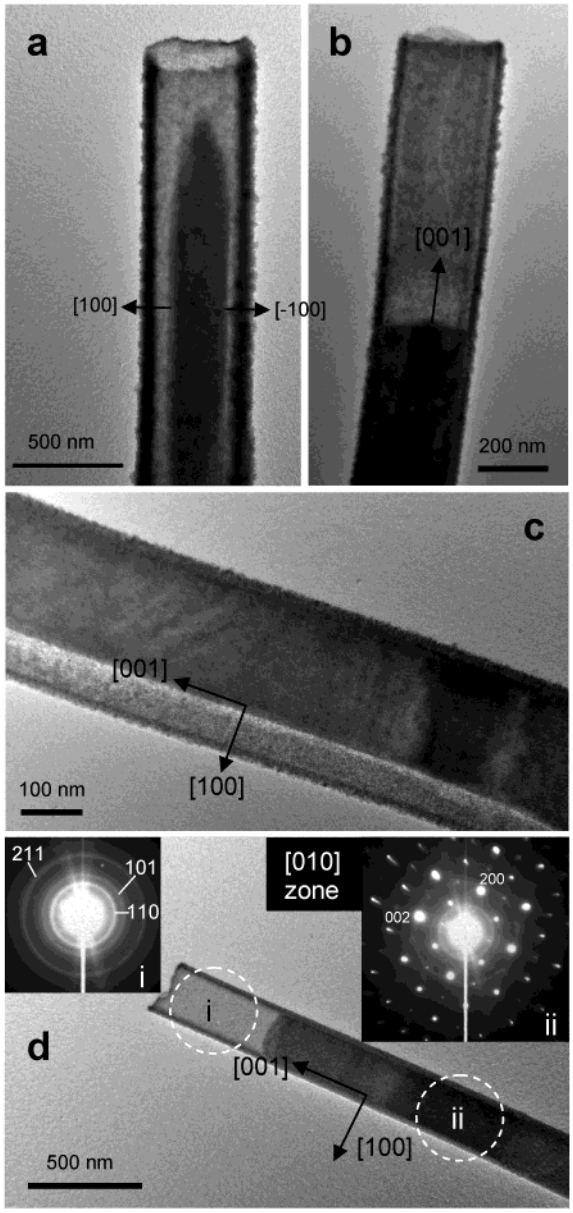

Figure 8. Dissolution modes of α-MoO_3 templates (a) from two sides, (b) from the top, and (c) from one side. (d) SAED patterns for the hollow area (numbered "i") and the SnO_2 sheathed part (numbered "ii") of a forming nanotube. Coordinate system is for the sheathed α-MoO_3 nanorod template viewed along the [010] axis of the crystal (refer to Figure 1).

on the first layer of the nanocrystallites that are in contact with the α-MoO_3 substrate.

In addition to the above hydrothermal methods, the SnO_2 shells can also be deposited on the α-MoO_3 templates under normal atmospheric pressure at 25−100 °C. As shown in Figure 10a, the SnO_2 sheathed α-MoO_3 nanorods could actually be prepared at room temperature (the final pH was around 1.6)! However, due to the low-temperature preparation, less thermal strains were generated, resulting in less cracking. For those with an open end (e.g., Figure 10b), the same dissolution modes as those of Figure 8 can also be found. In Figure 10c, for example, an analysis on the two SAED patterns similar to those reported for Figure 8d can be performed for the hollow and sheathed parts, respectively. Although less shell cracking was observed among the low temperature synthesized samples, evacuation of the solid α-MoO_3 templates can be accelerated with a post-

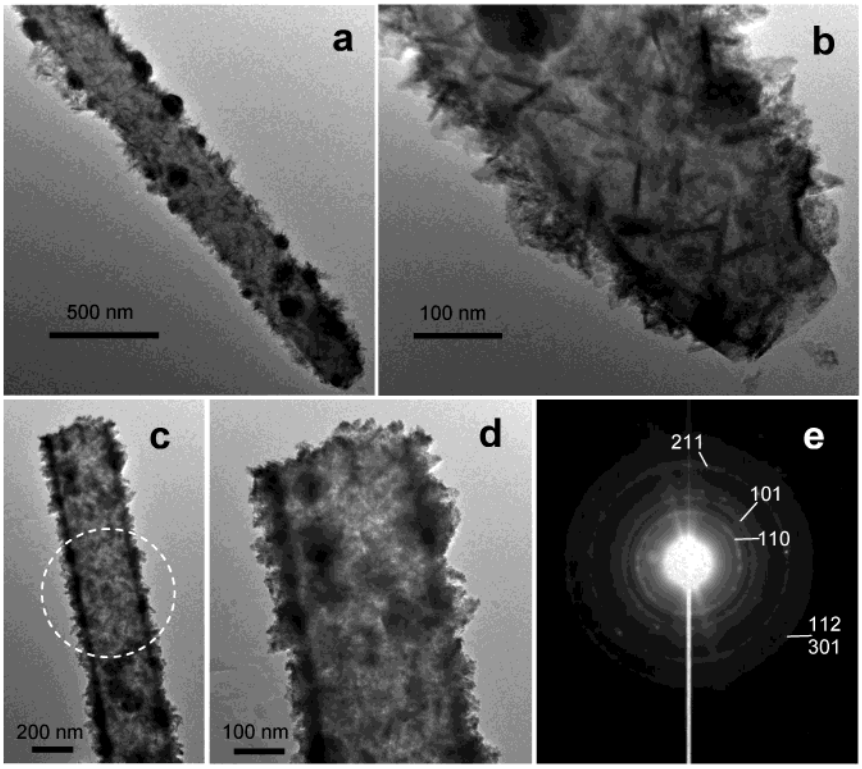

Figure 9. Texture investigation (TEM images and SAED) on SnO_2 nanotubes synthesized without using acids: (a) closed-ended SnO_2 nanotube with large crystallites on surface; (b) detailed view on the end part of (a); (c) open-ended SnO_2 nanotube; (d) detailed view on the end part of (c); (e) SAED pattern of the circled portion of (c). Synthetic conditions: 0.1 g of α-MoO_3 nanorods + 30 mL of H_2O + 1 g of Na_2SO_4 + 0.2 g of $SnCl_2{\cdot}2H_2O$ at 180 °C for 20 h.

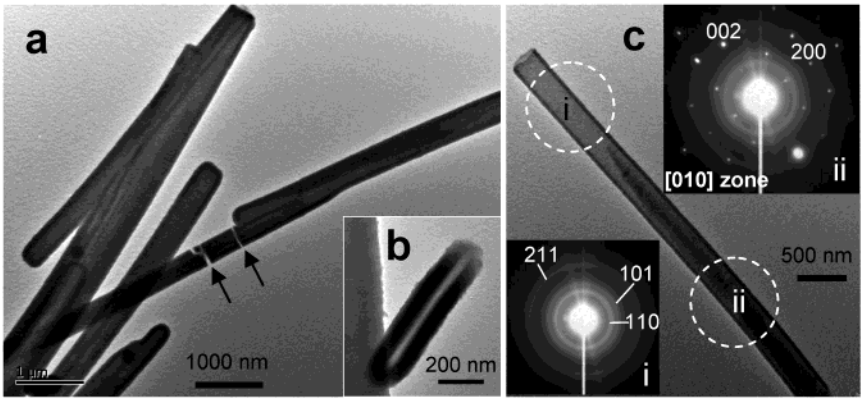

Figure 10. TEM and SAED investigations on SnO_2 nanotubes synthesized at room temperature: (a) SnO_2 sheathed α-MoO_3 (or H*x*MoO_3) nanorods; (b) short SnO_2 nanotube viewed along the side wall; (c) SAED patterns for the hollow area (numbered "i") and the SnO_2 sheathed part (numbered "ii") of a forming nanotube. Synthetic conditions: 0.1 g of α-MoO_3 nanorods + 50 mL of H_2O + 2 g of Na_2SO_4 + 2 mL of HCl solution (4 M) + 0.2 g of $SnCl_2{\cdot}2H_2O$ at room temperature for 24 h. Arrows indicate the cracking areas of the SnO_2 skins and naked α-MoO_3 nanorods.

growth treatment in dilute NaOH solution; note that the α-MoO_3 is an acidic transition metal oxide.[49] Under the basic condition, the α-MoO_3 in these sheathed samples can be completely removed, as demonstrated in Figure 11. Owing to the slow growth at low temperature, the quality of these nanotubes is comparable to that of those prepared under hydrothermal conditions but with higher contents of acid (e.g., Figures 2 and 3), as shown in the homogeneous crystallite grains on the shells of the nanotubes (Figure 11d). Furthermore, no autoclave was needed in the low-temperature synthesis, which allowed us to make a direct observation of the reaction processes. Since there was no gas evolving from the solution phase, it is suggestive that the formation of solid SnO_2 is likely through eq 2.[18,34,35] Similar to those in hydrothermal reactions, formation rates of solid SnO_2 at 25−100 °C (under normal atmosphere) are also very low, which is evidenced by the lack of spontaneous nucleation and growth of unsupported SnO_2 nanoparticles. In general, the high-temperature method forms stronger nanotubes and allows a rapid evacuation of α-MoO_3 templates owing to the fast reactions. On the other hand, the low-temperature method produces thinner tube walls and finer crystallites in the sheaths. Therefore, the two methods are actually complementary, depending on the product requirements.

Very recently, uniform SnO_2 nanoparticles in tetragonal phase had been coated onto boron nitride (BN) and single-walled carbon nanotube surfaces, where no inorganic additives were required in the depositions.[34,35] In contrast to these results, in our current case, it is apparent that the addition of Na_2SO_4 salt is indispensable for the deposition of SnO_2 shells on α-MoO_3, although the exact roles of the salts are still unclear. However,

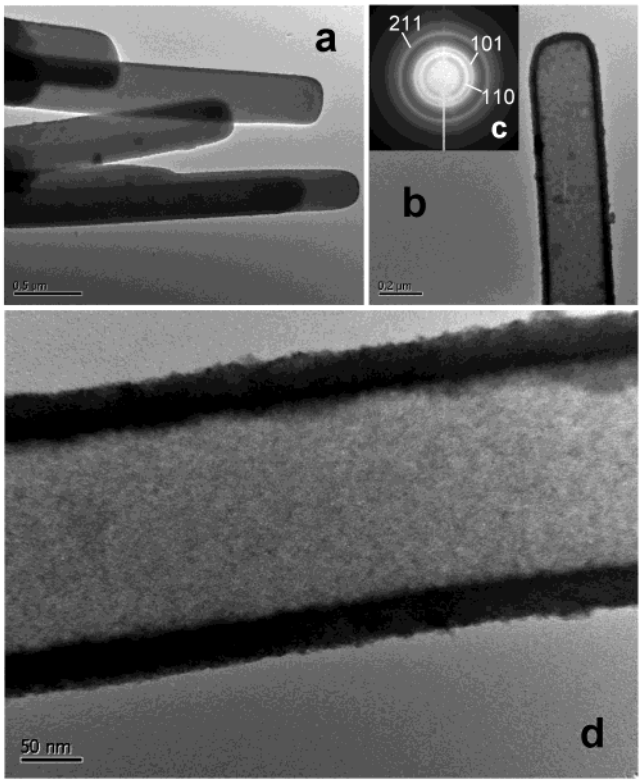

Figure 11. TEM and SAED investigations on SnO_2 nanotubes prepared with NaOH treatments: (a) SnO_2 sheathed α-MoO_3 nanorods before NaOH treatments; (b) SnO_2 nanotube after NaOH treatments; (c) SAED pattern for the tube in (b); (d) detailed view of the tube structure. Synthetic conditions: 0.1 g of α-MoO_3 nanorods + 40 mL of H_2O + 1 g of Na_2SO_4 + 1.5 mL of HNO_3 solution (4 M) + 0.2 g of $SnCl_2 \cdot 2H_2O$ at 100 °C for 4 h. NaOH treatments: 0.05 g of sample (a) + 9 mL of H_2O + 6 mL of NaOH solution (1 M), stirred for 10 min.

it is reasonable to assume that the salt may play two roles in the synthesis. First, it creates an ionic effect (e.g., adsorption of sulfate ions) to initiate heterogeneous nucleation on the surface of the α-MoO_3 nanorods. Second, it prevents the nanocrystallites of the shells from growing into large ones. In the absence of this salt, direct dissolution of α-MoO_3 nanorods has been observed instead of forming the SnO_2 shells. To further address this salt effect, other inorganic and organic salts have also been tested in this work. For example, addition of $NaNO_3$ does not promote the growth of SnO_2 sheaths, but does promote the formation of nanoparticles, which is also accompanied by the direct dissolution of α-MoO_3 nanorods. On the other hand, addition of C_2H_5COONa does promote the formation of SnO_2 shells, but the quality of the shells seems to be poorer due to easy formation of unattained nanoparticles as a separate secondary phase.

To estimate the optical energy band gap for SnO_2 nanotubes, a classical Tauc approach was employed in this work. It has been found that $n = 1/2$ (allowed direct transition) gives a best description of our ultraviolet absorption measurements. Figure 12 shows a representative plot of $(\alpha E_{photon})^2$ versus E_{photon} for a direct transition. The extrapolated value (the straight line) of E_{photon} at $\alpha = 0$ gives an absorption edge energy which corresponds to a band gap energy $E_g = 3.92$ eV. In agreement with the small crystallite sizes (~4 nm) observed with HRTEM for the SnO_2 shells, this value indicates a significant blue shift (0.30 eV) from the band gap energy of bulk tetragonal SnO_2 ($E_g = 3.62$ eV),[50] owing to the quantum confinement effects. Our E_g value is also in excellent agreement with the literature

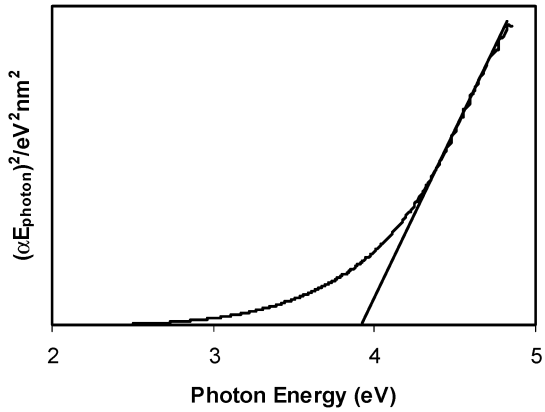

Figure 12. Plot of $(\alpha E_{photon})^2$ versus E_{photon} for the direct transition. Band gap energy of SnO_2 nanotubes obtained by extrapolation to $\alpha = 0$. Sample used in this measurement is from Figure 11 (average crystallite size is ~4 nm).

data for the SnO_2 nanocrystallites prepared with a high-temperature route (5.9 nm, $E_g = 3.65$ eV; 3.5 nm, $E_g = 3.97$ eV).[9]

The polycrystalline SnO_2 nanotubes prepared in this work can also be visualized as an organization of SnO_2 nanocrystallites with internal and external surfaces, or unsupported thin films (having double surfaces) comprised of nanocrystallites. In view of this special structural arrangement, insertion reactions could be more efficiently conducted with the tubularly organized SnO_2 nanocrystallites. For example, intercalation and deintercalation of alkali metals for secondary battery applications might benefit from this type of SnO_2 nanostructures (as an anode material), because volumetric expansion during the ionic insertion can be better accommodated with interstitials among the nanocrystallites. In this sense, polycrystalline nanotubes might be even more advantageous than their single-crystalline counterparts. Many research opportunities for the polycrystalline SnO_2 nanotubes are laid ahead. For example, our future research will be directed toward investigation of lithium insertion with these nanotube products, in analogy to those using carbon nanotubes.

Conclusions

In summary, we have developed a salt-assisted deposition method for fabrication of polycrystalline SnO_2 nanotubes with tetragonal crystallographic symmetry. Using α-MoO_3 nanorods, uniform nanocrystallites of SnO_2 with random orientations can be first deposited under normal atmospheric pressure (room temperature to 100 °C) or hydrothermal conditions (180 °C), followed by α-MoO_3 dissolution. The final tube shape preserves the original crystal morphology of α-MoO_3 templates, while the crystalline texture of the tubes can be further tailored. It has been proven that salt additives such as Na_2SO_4 are indispensable for the SnO_2 deposition. The optical band gap determined for the nanotubes is 3.92 eV (for crystallites with an average size of ~4 nm). This simple template method promises large-scale production of free-standing polycrystalline SnO_2 nanotubes with both structural engineering and crystallite size control.

Acknowledgment. The authors gratefully acknowledge research funding supported by the Ministry of Education, Singapore.

Supporting Information Available: HRTEM, EDX, and XRD results of tetragonal SnO_2 nanotubes as well as of their

undissolved templates. This material is available free of charge via the Internet at http://pubs.acs.org.

References and Notes

(1) (a) Rao, C. N. R.; Cheetham, A. K. *J. Mater. Chem.* **2001**, *11*, 2887. (b) Rao, C. N. R.; Kulkarni, G. U.; Thomas, P. J.; Edwards, P. P. *Chem. Eur. J.* **2002**, *8*, 29. (c) Rao, C. N. R.; Nath, M. *Dalton Trans.* **2003**, 1.

(2) Patzke, G. R.; Krumeich, F.; Nesper, R. *Angew. Chem., Int. Ed.* **2002**, *41*, 2446.

(3) Kovtyukhova, N. I.; Mallouk, T. E. *Chem. Eur. J.* **2002**, *8*, 4355.

(4) Xia, Y.; Yang, P.; Sun, Y.; Wu, Y.; Mayers, B.; Gates, B.; Yin, Y.; Kim, F.; Yan, H. *Adv. Mater.* **2003**, *15*, 353.

(5) Nayral, C.; Ould-Ely, T.; Maisonnat, A.; Chaudret, B.; Fau, P.; Lescouzères, L.; Peyre-Lavigne, A. *Adv. Mater.* **1999**, *11*, 61.

(6) He, Y.; Li, Y.; Yu, J.; Qian, Y. *Mater. Lett.* **1999**, *40*, 23.

(7) Zhu, J.; Lu, Z.; Aruna, S. T.; Aurbach, D.; Gedanken, A. *Chem. Mater.* **2000**, *12*, 2557.

(8) Leite, E.; Weber, I. T.; Longo, E.; Varela, J. A. *Adv. Mater.* **2000**, *12*, 965.

(9) Pang, G.; Chen, S.; Koltypin, Y.; Zaban, A.; Feng, S.; Gedanken, A. *Nano Lett.* **2001**, *1*, 723.

(10) Aurbach, D.; Nimberger, A.; Markovsky, B.; Levi, E.; Sominski, E.; Gedanken, A. *Chem. Mater.* **2002**, *14*, 4155.

(11) Broussous, L.; Santilli, C. V.; Pulcinelli, S. H.; Craievich, A. F. *J. Phys. Chem. B* **2002**, *106*, 2855.

(12) Zhu, J.-J.; Zhu, J.-M.; Liao, X.-H.; Fang, J.-L.; Zhou, M.-G.; Chen, H.-Y. *Mater. Lett.* **2002**, *53*, 12.

(13) Ristić, M.; Ivanda, M.; Popović, S.; Musić, S. *J. Non-Cryst. Solids* **2002**, *303*, 270.

(14) Deng, H.; Lamelas, F. J.; Hossenlopp, J. M. *Chem. Mater.* **2003**, *15*, 2429.

(15) Bhagwat, M.; Shah, P.; Ramaswamy, V. *Mater. Lett.* **2003**, *57*, 1604.

(16) Gu, F.; Wang, S. F.; Song, C. F.; Lü, M. K.; Qi, Y. X.; Zhou, G. J.; Xu, D.; Yuan, D. R. *Chem. Phys. Lett.* **2003**, *372*, 451.

(17) Zheng, M.; Li, G.; Zhang, X.; Huang, S.; Lei, Y.; Zhang, L. *Chem. Mater.* **2001**, *13*, 3859.

(18) Kijima, T.; Ikeda, T.; Yada, M.; Machida, M. *Langmuir* **2002**, *18*, 6453.

(19) Zhang, R.-Q.; Lifshitz, Y.; Lee, S.-T. *Adv. Mater.* **2003**, *14*, 1029.

(20) Kolmakov, A.; Zhang, Y.; Cheng, G.; Moskovits, M. *Adv. Mater.* **2003**, *15*, 997.

(21) Dai, Z. R.; Pan, Z. W.; Wang, Z. L. *Solid State Commun.* **2001**, *118*, 351.

(22) Wang, Z. L.; Pan, Z. *Adv. Mater.* **2002**, *14*, 1029.

(23) Hu, J. Q.; Ma, X. L.; Shang, N. G.; Xie, Z. Y.; Wong, N. B.; Lee, C. S.; Lee, S. T. *J. Phys. Chem. B* **2002**, *106*, 3823.

(24) Peng, X. S.; Zhang, L. D.; Meng, G. W.; Tian, Y. T.; Lin, Y.; Geng, B. Y.; Sun, S. H. *J. Appl. Phys.* **2003**, *93*, 1760.

(25) Hu, J. Q.; Bando, Y.; Golberg, D. *Chem. Phys. Lett.* **2003**, *372*, 758.

(26) Liu, Y.; Zheng, C.; Wang, W.; Yin, C.; Wang, G. *Adv. Mater.* **2001**, *13*, 1883.

(27) Xu, C.; Xu, G.; Liu, Y.; Zhao, X.; Wang, G. *Scr. Mater.* **2002**, *46*, 789.

(28) Dai, Z. R.; Gole, J. L.; Stout, J. D.; Wang, Z. L. *J. Phys. Chem. B* **2002**, *106*, 1274.

(29) Zhang, D.-F.; Sun, L.-D.; Yin, J.-L. Yan, C.-H. *Adv. Mater.* **2003**, *15*, 1022.

(30) Xu, C.; Zhao, X.; Liu, S.; Wang, G. *Solid State Commun.* **2003**, *125*, 301.

(31) Dai, Z. R.; Pan, Z. W.; Wang, Z. L. *J. Am. Chem. Soc.* **2002**, *124*, 8673.

(32) Wang, Z. L. *Adv. Mater.* **2003**, *15*, 432.

(33) Németh, J.; Dékány, I.; Süvegh, K.; Marek, T.; Klencsár, Z.; Vértes, A.; Fendler, J. H. *Langmuir* **2003**, *19*, 3762.

(34) Han, W.-Q.; Zettl, A. *J. Am. Chem. Soc.* **2003**, *125*, 2062.

(35) Han, W.-Q.; Zettl, A. *Nano Lett.* **2003**, *3*, 681.

(36) Zhong, Z.; Yin, Y.; Gates, B.; Xia, Y. *Adv. Mater.* **2000**, *12*, 206.

(37) Srivastava, D. N.; Chappel, S.; Palchik, O.; Zaban, A.; Gedanken, A. *Langmuir* **2002**, *18*, 4160.

(38) Zhou, S.; Lu, S.; Ke, Y.; Li, J. *Mater. Lett.* **2003**, *57*, 2679.

(39) Miyata, H.; Itoh, M.; Watanabe, M.; Noma, T. *Chem. Mater.* **2003**, *15*, 1334.

(40) Iijima, S. *Nature* **1991**, *354*, 56.

(41) (a) Ebbesen, T. W.; Ajayan, P. M. *Nature* **1992**, *358*, 220. (b) Ajayan, P. M.; Ebbesen; T. W. *Rep. Prog. Phys.* **1997**, *60*, 1025.

(42) Thess, A.; Lee, R.; Nikolaev, P.; Dai, H.; Petit, P.; Robert, J.; Xu, C.; Lee, Y. H.; Kim, S. G.; Rinzler, A. G.; Colbert, D. T.; Scuseria, G. E.; Tomanek, D.; Fischer, J. E.; Smalley, R. E. *Science* **1996**, *273*, 483.

(43) (a) Tenne, R.; Homyonfer, M.; Feldman, Y. *Chem. Mater.* **1998**, *10*, 3225. (b) Zak, A.; Feldman, Y.; Alperovich, V.; Rosentsveig, R.; Tenne, R. *J. Am. Chem. Soc.* **2000**, *122*, 11108. (c) Feldman, Y.; Frey, G. L.; Homyonfer, M.; Lyakhovitskaya, V.; Margulis, L.; Cohen, H.; Hodes, G.; Hutchison, J. L.; Tenne, R. *J. Am. Chem. Soc.* **1996**, *118*, 5362.

(44) Nath, M.; Rao, C. N. R. *J. Am. Chem. Soc.* **2001**, *123*, 4841.

(45) Lou, X. W.; Zeng, H. C. *Chem. Mater.* **2002**, *14*, 4781.

(46) Sampanthar, J. T.; Zeng, H. C. *J. Am. Chem. Soc.* **2002**, *124*, 6668.

(47) Cotton, F. A.; Wilkinson, G. *Advanced Inorganic Chemistry*, 4th ed.; John Willey & Sons: New York, 1980; Chapter 22, p 852.

(48) (a) Zeng, H. C. *Inorg. Chem.* **1998**, *37*, 1967. (b) Zeng, H. C.; Ng, W. K.; Cheong, L. H.; Xie, F.; Xu, R. *J. Phys. Chem. B* **2001**, *105*, 7178. (c) Zeng, H. C.; Xie, F.; Wong, K. C.; Mitchell, K. A. R. *Chem. Mater.* **2002**, *14*, 1788.

(49) Lou, X. W.; Zeng, H. C. *J. Am. Chem. Soc.* **2003**, *125*, 2697.

(50) (a) Aoki, A.; Sasakura, H. *Jpn. J. Appl. Phys.* **1970**, *9*, 582. (b) Tatsuyama, C.; Ichimura, S. *Jpn. J. Appl. Phys.* **1976**, *15*, 843.